ROYAL SOCIETY
OF CHEMISTRY

PAPER

Check for updates

Synthesis of a pyridine-based covalent organic framework as an efficient adsorbent for rhodamine B removal†

Kejian Chang, [ID] * Huijuan Huang, Yuandong Meng, Zidan Ju, Haiyan Song, Liang Zhang, [ID] Xiaoqin Niu and Zhi-Jun Li [ID] *

Covalent organic frameworks (COFs), featured with crystalline structures, permanent porosity, and designable organic skeletons, are good candidates for serving as adsorbents. Herein, a new pyridine-based two-dimensional COF (TAPP-DBTA-COF) was constructed via the condensation of 2,4,6-tris(4-aminophenyl)pyridine and 2,5-dibromobenzene-1,4-dicarbaldehyde. TAPP-DBTA-COF displayed high-performance for the removal of rhodamine B (Rh B) from water with high capacity, good adaptability and reusability. The maximum adsorption capacity for Rh B can reach up to 1254 mg g^{-1}, and the kinetic constant was determined as $k_2 = 0.00244$ g mg^{-1} min^{-1}. Moreover, the corresponding amorphous polymer of TAPP-DBTA-COF, termed as TAPP-DBTA-COP, was synthesized from the same starting materials. The lower efficiency of TAPP-DBTA-COP in capture of Rh B revealed that the ordered pore structure, large specific surface area and rich adsorption sites play an important role in adsorption.

Introduction

Rapid industrialization has led to the appearance of a large amount of industrial pollutants, most of which were discharged directly to environment without appropriate treatment.[1] As some of the most common industrial pollutants in water, organic dyes are highly water-soluble, stable and highly resistant to degradation.[2–4] Release of organic dyes into the environment has caused tremendous threats to living organisms and human health due to their toxicity and carcinogenicity.[5] It is of vital significance to explore effective, sustainable, economical and environmentally friendly strategies to treat dye-containing wastewater.[6]

Adsorption has the advantages of high efficiency, low cost and convenient operation. Therefore, development of high-performance adsorbents is highly desirable for water decontamination.[7,8] In the past decades, considerable attention has been paid to the exploration of various advanced porous materials, such as zeolites,[9,10] activated carbon,[11] metal organic frameworks (MOFs),[12–14] and covalent organic polymers (COPs).[15] These materials have been applied to various pollutants removal from water. However, most of these sorbents suffer from poor selectivity and limited adsorption capacity due to their intrinsic structure features (e.g. lack of functionality for

College of Petrochemical Engineering, Longdong University, Qingyang, Gansu, 745000, P. R. China. E-mail: kejianchang_chem@163.com; lizhj_chem@163.com

zeolites, limited tunability for activated carbon), which greatly limited their application in water decontamination.[16]

Covalent organic frameworks (COFs), an emerging class of crystalline materials,[17–20] featuring ordered skeletons, low density, high stability, large specific surface area and designable pore functionality,[21] have been applied in diverse fields, including gas storage and separation,[22,23] sensors,[24–26] heterogeneous catalysis,[27–33] drug delivery,[34,35] pollutant treatment,[36–40] etc. It has been verified that COFs, especially integrating with specific functional groups, have great potential as adsorbents in pollutants removal.[41–47] For example, Zhu et al. reported a triazine-functionalized TS-COF-1 that exhibited high efficiency in the adsorption of methylene blue (MB) with a maximum adsorption capacity of ~1691 mg g^{-1}.[48] In particular, efficient nitrogen sites derived from the triazine group and C=N unit play a significant role in the electrostatic interaction between the COFs and MB molecules. Likewise, Xu et al. developed a triazine-based Ttba-TPDA-COF which exhibited an impressive adsorption capacity of ~833 mg g^{-1} for removal of Rh B.[49] Additionally, Fang et al. reported that amide-functionalized two-dimensional COF (JUC-578) can selectively adsorb cationic dyes.[50] These examples proved that COFs are ideal candidates as adsorbents for water decontamination. However, the development of COFs as adsorbents in dyes removal is still at the early stage and only a few studies were reported so far.[51] Therefore, there is an urgent need to develop new COFs with efficient and selective dyes adsorption ability.

The number of active sites is crucial structural factor affecting the capacity of adsorbents in dyes adsorption. It has been demonstrated that the introduction of nitrogen-
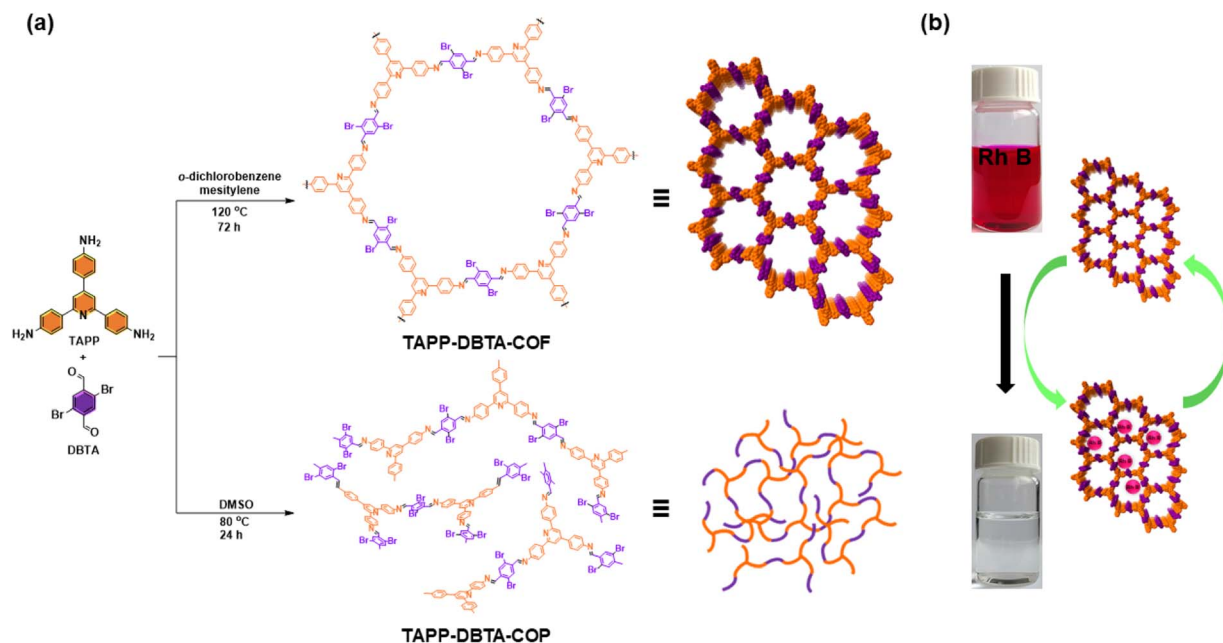
Fig. 1 (a) Synthesis of TAPP-DBTA-COF and TAPP-DBTA-COP by the Schiff base condensation under different conditions. (b) Schematic representation for the adsorption of Rh B by TAPP-DBTA-COF.

containing functional groups into COFs can provide abundant active sites for dyes adsorption by electrostatic interactions.[48,49,51] Encouraged by this, we envisioned that the introduction of pyridine unit in monomer can effectively increase the accessible adsorption sites in the frameworks, thus improving the adsorption capacity of COFs. Therefore, in this work, we described the design and synthesis of a novel pyridine-based two-dimensional COF (TAPP-DBTA-COF) through Schiff-based condensation reaction of 2,4,6-tris(4-aminophenyl)pyridine and 2,5-dibromobenzene-1,4-dicarbaldehyde. Owing to the high crystallinity, large BET surface area and abundant adsorption sites, TAPP-DBTA-COF exhibited an excellent performance for removal of Rh B from water with a maximum adsorption capacity of up to 1254 mg g^{-1} (Fig. 1). Meanwhile, the corresponding amorphous polymer TAPP-DBTA-COP was synthesized and applied to Rh B removal. The adsorption performance of TAPP-DBTA-COF was far superior to that of TAPP-DBTA-COP. These results demonstrate that the ordered pore structure, large specific surface area and rich adsorption sites are crucial factors to adsorbents and TAPP-DBTA-COF has a great application potential in dye removal and water purification.

Experimental

Synthesis of TAPP-DBTA-COF

2,4,6-Tris(4-aminophenyl)pyridine (188 mg, 0.5 mmol), 2,5-dibromobenzene-1,4-dicarbaldehyde (233 mg, 0.8 mmol) and 6 mL o-dichlorobenzene/mesitylene (4 mL/2 mL) were charged into a 20 mL vial. The resulting mixture was sonicated for 5 min and then 0.8 mL of 6 M acetic acid was added. The vial was

sealed and heated at 120 °C for 72 h. The precipitate was collected by filtration and washed with dichloromethane, acetone, methanol respectively. Further purification was conducted via Soxhlet extraction with THF for 12 h. After being dried at 80 °C for 10 h, the final TAPP-DBTA-COF was obtained as a yellow powder in 85% yield. Elemental analysis: calcd for $C_{70}H_{40}N_8Br_6$: C, 57.10; H, 2.74; N, 7.61. Found: C, 56.04; H, 2.64; N, 7.89.

Synthesis of TAPP-DBTA-COP

2,4,6-Tris(4-aminophenyl)pyridine (106 mg, 0.30 mmol), 2,5-dibromobenzene-1,4-dicarbaldehyde (131 mg, 0.45 mmol) and 8 mL DMSO were charged into a 50 mL vial. The resulting mixture was heated at 80 °C for 24 h. After that, the precipitate was collected by filtration and washed with dichloromethane, acetone, methanol respectively. Further purification was conducted via Soxhlet extraction with THF for 12 h. After being dried at 80 °C for 10 h, the final TAPP-DBTA-COP was obtained as a pale brown powder in 83% yield. Elemental analysis: calcd for $C_{70}H_{40}N_8Br_6$: C, 57.10; H, 2.74; N, 7.61. Found: C, 55.72; H, 2.82; N, 7.92.

Sorption kinetics study

Typically, TAPP-DBTA-COF or TAPP-DBTA-COP (3 mg) was dispersed in 5 mL Rh B aqueous solution (200 ppm) and stirred under room temperature. After stirring for a desired time, the sorbent was filtered with a syringe filter (PTFE, 0.45 μm), and the solution was detected by UV-vis spectrophotometer. The adsorption percentage was obtained by comparing the maximum absorbance (λ = 554 nm) with the original Rh B aqueous solution.

Sorption isotherm study

The sorption isotherm experiments of TAPP-DBTA-COF and TAPP-DBTA-COP were conducted by varying the initial concentrations of Rh B. Typically, adsorbent (5 mg) was dispersed in 6 mL Rh B aqueous solution. The solution was stirred for 2.5 h under room temperature, and then the solution was filtered with a syringe filter (PTFE, 0.45 μm). After being diluted with deionized water, the solution was measured with UV-vis spectrophotometer. The maximum adsorption capacity (Q_m) was calculated from the adsorption isotherm.

The influence of pH value of the solution was studied by dispersing TAPP-DBTA-COF (5 mg) in 6 mL Rh B aqueous solution (1400 ppm) with different pH values (pH = 1, 3, 7, 9, 12). The pH values of the solution were adjusted *via* adding 0.1 M HCl or 0.1 M NaOH. After stirring for 2 hours, the sorbent was filtered with a syringe filter (PTFE, 0.45 μm), and the solutions were detected by UV-vis spectrophotometer, the adsorption percentage was determined based on the intensity reduction of the characteristic peak of Rh B.

The recyclability of TAPP-DBTA-COF was studied in an amplified experiment. 28 mg of TAPP-DBTA-COF was dispersed in 40 mL Rh B aqueous solution (1400 ppm), and stirred for adsorption. The adsorbed Rh B can be desorbed *via* directly eluting with ethanol until the eluent was changed to colorless. The ethanol solution was collected and detected by UV-vis spectrophotometer to determine desorption efficiency. After thoroughly washing with ethanol, the regenerated adsorbent TAPP-DBTA-COF-Regenerated was obtained and dried at 80 °C. The next adsorption cycle was performed under the same conditions.

Results and discussion

Synthesis and characterization

We selected 2,4,6-tris(4-aminophenyl)pyridine (TAPP)[52] as node and 2,5-dibromobenzene-1,4-dicarbaldehyde (DBTA)[53] as linker to synthesize TAPP-DBTA-COF through the Schiff base condensation reaction under solvothermal conditions (Fig. 1a). The reaction was conducted in a mixed solvent of *o*-dichlorobenzene/mesitylene at 120 °C for 72 h in the presence of 6 M acetic acid. TAPP-DBTA-COF was successfully obtained as a yellow powder. During the synthesis of materials, the solvent effect is undoubtedly very important and exerts significant influence on the nucleation, growth and assembly of the polymeric intermediates.[54,55] Accordingly, starting from the same materials, TAPP-DBTA-COP was synthesized in DMSO at 80 °C for 24 h as a pale brown powder (Fig. 1a). Both TAPP-DBTA-COF and TAPP-DBTA-COP are stable and insoluble in common organic solvents, such as tetrahydrofuran (THF), acetone, ethanol, and dimethyl sulfoxide (DMSO). Fourier transform infrared (FT-IR) spectroscopy was conducted to confirm the formation of C=N bond. TAPP-DBTA-COF and TAPP-DBTA-COP exhibited analogous FT-IR spectra in which the characteristic signal at 1595 cm^{-1} was attributed to the C=N group in both materials (Fig. 2a). Meanwhile, the peaks of the CHO group at 1685 cm^{-1} and the NH$_2$ group at 3256 cm^{-1} in starting materials almost disappeared, suggesting the successful condensation between CHO and NH$_2$ groups (Fig. S1†). The chemical structures of TAPP-DBTA-COF and TAPP-DBTA-COP were also determined by the solid-state ^{13}C CP-MAS in which the C=N linkage was located at 154 ppm (Fig. 2c).

X-ray powder diffraction (PXRD) and theoretical simulation experiments were performed to evaluate the crystalline structure of TAPP-DBTA-COF and TAPP-DBTA-COP. As shown in Fig. 2b, TAPP-DBTA-COF displayed strong PXRD peaks, indicating an excellent crystallinity. Conversely, the PXRD patterns of TAPP-DBTA-COP exhibited a broad reflection around 25°, which demonstrated its amorphous structure (Fig. S2†). Materials Studio (2019 (19.1.0.2353) version) was used to simulate powder diffraction patterns of COF structures and perform Pawley refinements. The TAPP-DBTA-COF adopted the AA stacking mode with the monoclinic unit cell of parameters a = 38.7109 Å, b = 3.5765 Å, c = 35.7454 Å, $β$ = 117.4762°, R_{wp} = 6.90%, R_p = 5.29%. The experimental PXRD patterns matched very well with the simulated PXRD patterns of the eclipsed (AA) stacking mode. Furthermore, the morphologies of TAPP-DBTA-COF and TAPP-DBTA-COP were examined by scanning electron microscopy (SEM). TAPP-DBTA-COF presented a reticular and porous morphology while TAPP-DBTA-COP displayed irregular agglomerate morphology (Fig. 3a and b). N$_2$ adsorption/desorption analyses were performed to provide insight into the porosity of TAPP-DBTA-COF and TAPP-DBTA-COP (Fig. 3c). The Brunauer–Emmett–Teller (BET) surface area of TAPP-DBTA-COF was calculated as 1578.4 m^2 g^{-1}, which was significantly higher than that of TAPP-DBTA-COP (115.9 m^2 g^{-1}) and was close to previously reported BrCOF-1 and BrCOF-2.[56] The N$_2$ sorption isotherms exhibited a sharp rise at low relative pressure and a hysteresis loop at high relative pressure, which illustrated that the pore structure nature of TAPP-DBTA-COF is comprised of abundant micropores and sufficient mesopores.[57,58] The pore size distributions revealed that TAPP-DBTA-COF adopted main peaks at around 2.8 nm (Fig. S3†). Thermogravimetric analysis (TGA) of TAPP-DBTA-COF and TAPP-DBTA-COP illustrated that two materials are similar in thermal stability and are stable up to 400 °C under N$_2$, suggesting a highly thermal stability (Fig. 3d). Furthermore, the chemical stability of TAPP-DBTA-COF was examined in different aqueous solutions (pH = 1–12) at 25 °C for 12 h. The PXRD patterns and N$_2$ sorption isotherms revealed that TAPP-DBTA-COF has a good chemical stability under neutral condition, and some loss of crystallinity and microporous structure was observed at pH = 1, 3, 9 & 12 (Fig. S8 and S9†).

Dye adsorption

Owing to the large surface area, high stability and regular channel pores with abundant nitrogen sites, TAPP-DBTA-COF is expected to be a promising candidate for dye adsorption. Rhodamine B (Rh B), a water-soluble cationic dye, has been widely used in the textile industry, leather, and other industries. However, the wastewater containing Rh B is highly toxic and carcinogenic to aquatic environment and human body.[49] Consequently, we use Rh B as an adsorbate to evaluate the
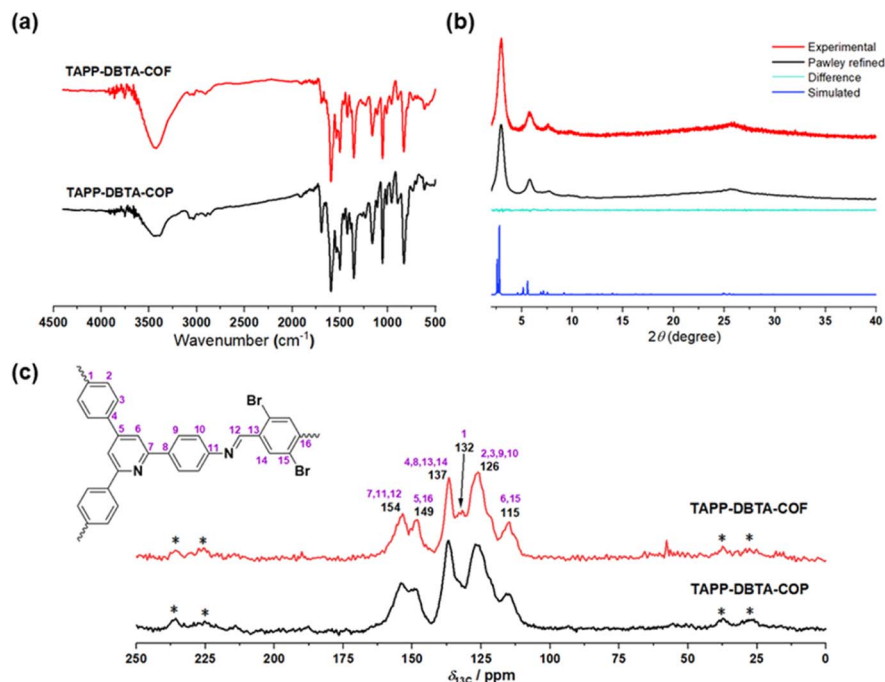
Fig. 2 (a) FT-IR spectra of TAPP-DBTA-COF and TAPP-DBTA-COP. (b) Powder XRD patterns of TAPP-DBTA-COF. (c) Solid-state ^{13}C CP-MAS NMR spectra of TAPP-DBTA-COF and TAPP-DBTA-COP.

adsorption performance of TAPP-DBTA-COF in water. In addition, to investigate the factors that influenced the adsorption behavior, we performed control experiments using TAPP-DBTA-COF and TAPP-DBTA-COP as the adsorbents. TAPP-DBTA-COP, which was prepared with the same starting materials used for TAPP-DBTA-COF, has poor crystallinity and a low BET surface area of 115.9 m^2 g^{-1}. Generally, 3 mg TAPP-DBTA-COF was dispersed in 5 mL Rh B aqueous solution (200 ppm) and stirred under ambient temperature for a certain time. After adsorption, the sorbent was separated with a syringe filter (poly(tetrafluoroethylene), 0.45 μm). UV-visible (UV-vis) absorption spectroscopy was employed to estimate dye adsorption efficiency. As
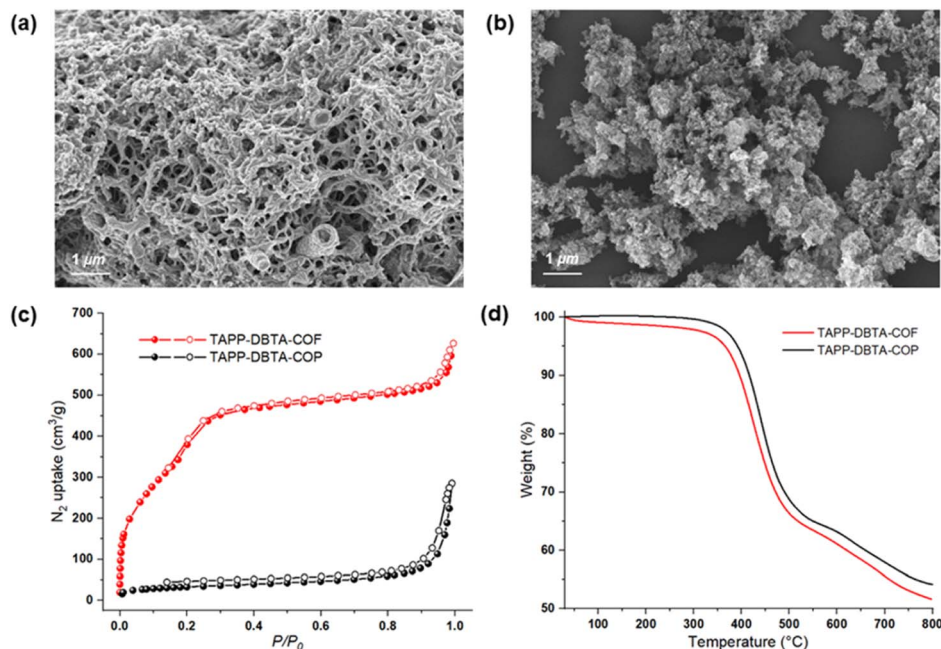

Fig. 3 SEM images of TAPP-DBTA-COF (a) and TAPP-DBTA-COP (b). Nitrogen sorption isotherm curves (c) and TGA curves (d) of TAPP-DBTA-COF and TAPP-DBTA-COP.

shown in Fig. 4a, 78% Rh B can be removed within only 4 min and 99% Rh B was removed in 30 min. For comparison, the adsorption kinetics of Rh B by TAPP-DBTA-COP were also performed (Fig. 4b). The pseudo-second-order kinetic model and pseudo-first-order kinetic model fits reasonably well with in both materials. The kinetics constants of TAPP-DBTA-COF ($k_2 = 0.00244$ g mg^{-1} min^{-1}) and TAPP-DBTA-COP ($k_2 = 0.00141$ g mg^{-1} min^{-1}) indicated that the adsorption of Rh B by two materials can reach an equilibrium value only several minutes (Fig. S10 and S11†). The poor adsorption capacity of TAPP-DBTA-COP illustrated that the adsorption mainly depends on accumulated pores and external surface adsorption, which is consistent with its low BET surface area (115.9 m^2 g^{-1}). Conversely, highly ordered porous structure, abundant porous channels and high specific surface area (1578.4 m^2 g^{-1}) endow TAPP-DBTA-COF with fast adsorption rate and excellent adsorption capacity.

Subsequently, we examined the maximum adsorption capacity of TAPP-DBTA-COF and TAPP-DBTA-COP by using various Rh B aqueous solutions with different concentrations. As observed in Fig. 4c, with an increase of equilibrium concentration of Rh B aqueous solutions, the adsorption capacity of two materials first rapidly rises and then tends to balance. The adsorption equilibrium data were fitted with LangmuirEXT1, Langmuir and Freundlich isotherm models to describe the interaction between TAPP-DBTA-COF and Rh B dye, and the corresponding parameters were listed. Obviously, LangmuirEXT1 isotherm model, which is a combination of Langmuir and Freundlich isotherm models and is more

advanced than these two isotherm models,[59] is more satisfactory in both cases in illustrating the adsorption of Rh B (Fig. S12 and S13†). Accordingly, the maximum adsorption capacities (Q_m) of TAPP-DBTA-COF and TAPP-DBTA-COP are calculated to be 1254 and 264 mg g^{-1}, respectively. The calculated Q_m values are in well agreement with the experimental values (1187 mg g^{-1} for TAPP-DBTA-COF and 219 mg g^{-1} for TAPP-DBTA-COP). Consequently, TAPP-DBTA-COF displayed excellent adsorption performance for Rh B than that of TAPP-DBTA-COP in both adsorption kinetic and isotherms studies. These results effectively clarified that ordered pore structure and large specific surface area of adsorbents have a profound impact on the adsorption of Rh B. Additionally, the adsorption capacity comparisons of previously reported adsorbents and TAPP-DBTA-COF for Rh B were summarized. As shown in Fig. 4d and Table 1, the adsorption capacity of TAPP-DBTA-COF surpassed most of other comparable adsorbents,[60–69] such as metal organic framework MIL-68(Al) (1111 mg g^{-1}),[61] covalent organic framework SCF-FCOF-1 (1044 mg g^{-1}),[44] ordered mesoporous carbon MPSC/C (785 mg g^{-1}),[62] hollow porous organic polymer h-COP-P (460 mg g^{-1}),[67] etc.

The influence of solution pH on the adsorption capacity is critical factor during the practical application and thus the Rh B adsorption efficiency of TAPP-DBTA-COF over a wide pH range was examined. As depicted in Fig. 4e, TAPP-DBTA-COF retained high adsorption capacity at pH 7 and exhibited decrease under acidic and basic environment, which is consistent with its chemical stability.
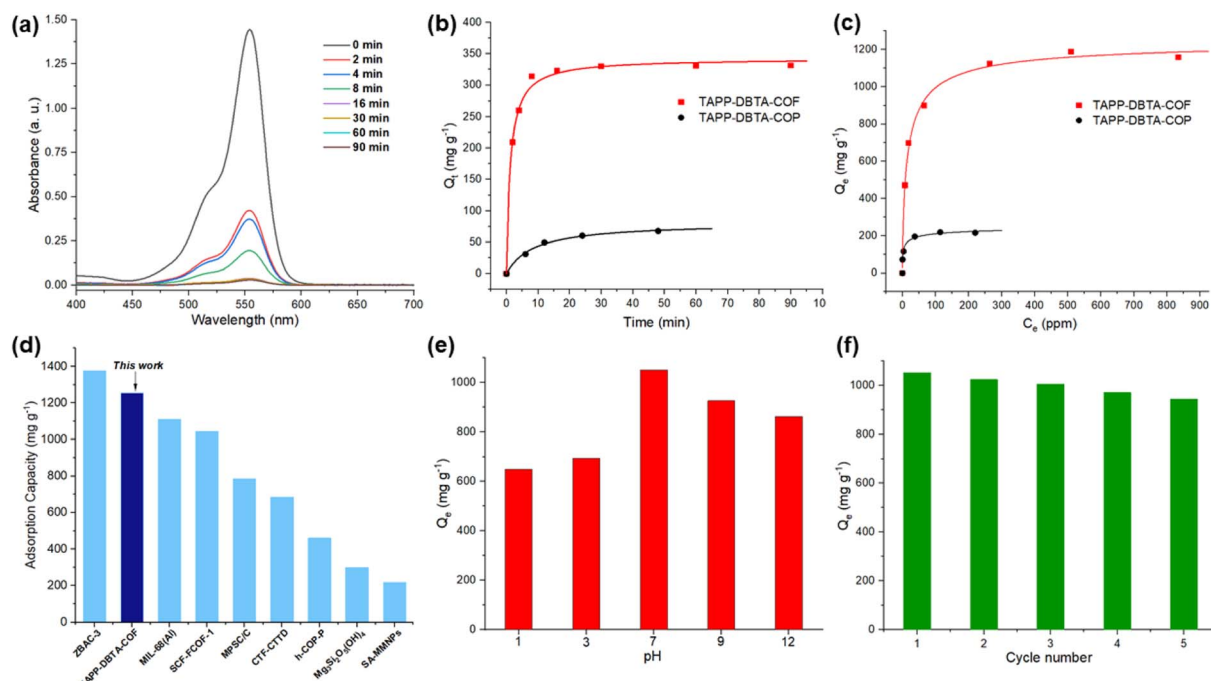

Fig. 4 (a) UV-vis spectra of a Rh B aqueous solution (200 ppm) in the presence of TAPP-DBTA-COF at different time intervals. Comparisons of the adsorption kinetics (b) and the adsorption isotherm (c) of Rh B by TAPP-DBTA-COF and TAPP-DBTA-COP. (d) Adsorption capacity comparisons of TAPP-DBTA-COF and other reported adsorbents. (e) Adsorption capacity of Rh B by TAPP-DBTA-COF at different pH values. (f) Recyclability of TAPP-DBTA-COF for adsorption of Rh B.

Table 1 Comparison of the BET surface area and adsorption performance of Rh B among various adsorbents

Adsorbents	S_{BET} (m^2 g^{-1})	Capacity [mg g^{-1}]	Ref.
ZBAC-3	1307	1375.8	60
TAPP-DBTA-COF	1578	1254	This work
MIL-68(Al)	976	1111	61
SCF-FCOF-1	2056	1044	44
Ttba-TPDA-COF	726	833	49
MPSC/C	2580	785	62
1-Eu	376	735	63
HHT-ZHT-[2]-P	1947	714	64
CTF-CTTD	1684	684.9	65
TS-COF-1	1484	625	66
h-COP-P	869	460	67
Mg$_3$Si$_2$O$_5$(OH)$_4$	281.68	300.08	68
SA-MMNPs	485	215.98	69

The reusability of adsorbents is crucial in the process of practical applications. Therefore, we examined the reusability of TAPP-DBTA-COF in an amplified experiment. Conveniently, the regeneration of TAPP-DBTA-COF could be rapidly realized by washing TAPP-DBTA-COF-Rh B with ethanol within few minutes. After drying, the regenerated adsorbent (TAPP-DBTA-COF-regenerated) can be used again under the same conditions. Desorption experiment showed that desorption efficiency of Rh B on TAPP-DBTA-COF with ethanol reached 97–98% and about 2–3% Rh B adsorbed are still trapped within porous network after each cycle (Fig. S14†). After five regeneration cycles, TAPP-DBTA-COF can maintain excellent adsorption capacity with little decrease (Fig. 4f). Furthermore, the regenerated TAPP-DBTA-COF retained chemical structure in comparison with freshly prepared TAPP-DBTA-COF, which was adequately evidenced by FT-IR spectroscopy (Fig. S15†). The PXRD pattern of TAPP-DBTA-COF-regenerated exhibited some loss of crystallinity and broadening of reflection pattern at high 2 theta, which may be caused by Rh B trapped within porous network (Fig. S16†). These excellent performance results demonstrated that TAPP-DBTA-COF possess an outstanding stability and reusability in the adsorption of Rh B and can be applied in water remediation as efficient adsorbents. Additionally, FT-IR spectroscopy was employed to analyze the changes of adsorbent before and after adsorption. As depicted in Fig. S17,† two new characteristic vibration peaks at 1755 cm^{-1} and 2966 cm^{-1} belonging to Rh B were observed after Rh B adsorption, which confirmed the successful adsorption of Rh B molecule on TAPP-DBTA-COF-Rh B. In contrast, with the desorption of Rh B, the peaks at 1755 cm^{-1} and 2966 cm^{-1} disappeared in TAPP-DBTA-COF-regenerated. The shifting of the characteristic stretching vibration band of C=N unit from 1595 cm^{-1} to 1591 cm^{-1} before and after adsorption indicated that the adsorption process involved the interaction between Rh B and TAPP-DBTA-COF. Furthermore, it is worth noting that TAPP-DBTA-COF contains abundant electron rich N atoms from pyridine and C=N units that could provide more accessible active sites for Rh B adsorption by electrostatic interactions,[48,49,51] which enables TAPP-DBTA-COF a high adsorption capacity.

Conclusions

In conclusion, we successfully synthesized a novel pyridine-based two-dimensional TAPP-DBTA-COF and an amorphous TAPP-DBTA-COP through Schiff-based condensation reaction of 2,4,6-tris(4-aminophenyl)pyridine and 2,5-dibromobenzene-1,4-dicarbaldehyde. Despite the similarity in chemical constitution, their properties vary markedly. TAPP-DBTA-COF, which has better crystallinity and larger BET surface area (1578.4 m^2 g^{-1}) than that of TAPP-DBTA-COP, exhibited an excellent performance for adsorption of Rh B with a maximum adsorption capacities of 1254 mg g^{-1}, as well as good adaptability and reusability. Significantly, further control experiments indicated that ordered pore structure, large specific surface area and abundant adsorption sites play an important role in the process of dyes adsorption. This study not only presents a high-performance COF adsorbent for water remediation but also gives new insights into the design of more advanced adsorbents.

Conflicts of interest

There are no conflicts to declare.

Acknowledgements

References

1 I. Ali, *Chem. Rev.*, 2012, **112**, 5073–5091.
2 S. Dutta, B. Gupta, S. K. Srivastava and A. K. Gupta, *Mater. Adv.*, 2021, **2**, 4497–4531.
3 V. Katheresan, J. Kansedo and S. Y. Lau, *J. Environ. Chem. Eng.*, 2018, **6**, 4676–4697.
4 C. X.-H. Su, L. W. Low, T. T. Teng and Y. S. Wong, *J. Environ. Chem. Eng.*, 2016, **4**, 3618–3631.
5 S. Bolisetty, M. Peydayesh and R. Mezzenga, *Chem. Soc. Rev.*, 2019, **48**, 463–487.
6 S. Samsami, M. Mohamadizaniani, M.-H. Sarrafzadeh, E. R. Rene and M. Firoozbahr, *Process Saf. Environ. Prot.*, 2020, **143**, 138–163.
7 G. Crini, *Bioresour. Technol.*, 2006, **97**, 1061–1085.
8 M. Shabir, M. Yasin, M. Hussain, I. Shafiq, P. Akhter, A.-S. Nizami, B.-H. Jeon and Y.-K. Park, *J. Ind. Eng. Chem.*, 2022, **112**, 1–19.
9 S. Wang and Y. Peng, *Chem. Eng. J.*, 2010, **156**, 11–24.

10 S. Wang and Z. H. Zhu, *J. Hazard. Mater.*, 2006, **136**, 946–952.

11 D. Mohan and C. U. Pittman, *J. Hazard. Mater.*, 2006, **137**, 762–811.

12 S. Rojas and P. Horcajada, *Chem. Rev.*, 2020, **120**, 8378–8415.

13 S. Zhang, J. Wang, Y. Zhang, J. Ma, L. Huang, S. Yu, L. Chen, G. Song, M. Qiu and X. Wang, *Environ. Pollut.*, 2021, **291**, 118076.

14 A. O. Ibrahim, K. A. Adegoke, R. O. Adegoke, Y. A. AbdulWahab, V. B. Oyelami and M. O. Adesina, *J. Mol. Liq.*, 2021, **333**, 115593.

15 T. Skorjanc, D. Shetty and A. Trabolsi, *Chem*, 2021, **7**, 882–918.

16 Y. Zhou, J. Lu, Y. Zhou and Y. Liu, *Environ. Pollut.*, 2019, **252**, 352–365.

17 A. P. Côté, A. I. Benin, N. W. Ockwig, M. O'keeffe, A. J. Matzger and O. M. Yaghi, *Science*, 2005, **310**, 1166–1170.

18 H. M. El-Kaderi, J. R. Hunt, J. L. Mendoza-Cortes, A. P. Côté, R. E. Taylor, M. O'keeffe and O. M. Yaghi, *Science*, 2007, **316**, 268–272.

19 S. Y. Ding and W. Wang, *Chem. Soc. Rev.*, 2013, **42**, 548–568.

20 P. J. Waller, F. Gándara and O. M. Yaghi, *Acc. Chem. Res.*, 2015, **48**, 3053–3063.

21 K. Geng, T. He, R. Liu, S. Dalapati, K. T. Tan, Z. Li, S. Tao, Y. Gong, Q. Jiang and D. Jiang, *Chem. Rev.*, 2020, **120**, 8814–8933.

22 S. S. Han, H. Furukawa, O. M. Yaghi and W. A. Goddard, *J. Am. Chem. Soc.*, 2008, **130**, 11580–11581.

23 P. Kuhn, M. Antonietti and A. Thomas, *Angew. Chem., Int. Ed.*, 2008, **47**, 3450–3453.

24 G. Lin, H. Ding, D. Yuan, B. Wang and C. Wang, *J. Am. Chem. Soc.*, 2016, **138**, 3302–3305.

25 W.-R. Cui, C.-R. Zhang, W. Jiang, F.-F. Li, R.-P. Liang, J. Liu and J.-D. Qiu, *Nat. Commun.*, 2020, **11**, 436.

26 Z. Meng and K. A. Mirica, *Chem. Soc. Rev.*, 2021, **50**, 13498–13558.

27 S. Y. Ding, J. Gao, Q. Wang, Y. Zhang, W. G. Song, C. Y. Su and W. Wang, *J. Am. Chem. Soc.*, 2011, **133**, 19816–19822.

28 Q. Fang, S. Gu, J. Zheng, Z. Zhuang, S. Qiu and Y. Yan, *Angew. Chem., Int. Ed.*, 2014, **53**, 2878–2882.

29 S. Lin, C. S. Diercks, Y.-B. Zhang, N. Kornienko, E. M. Nichols, Y. Zhao, A. R. Paris, D. Kim, P. Yang, O. M. Yaghi and C. J. Chang, *Science*, 2015, **349**, 1208–1213.

30 H. Xu, J. Gao and D. Jiang, *Nat. Chem.*, 2015, **7**, 905–912.

31 Q. Sun, B. Aguila, J. Perman, N. Nguyen and S. Ma, *J. Am. Chem. Soc.*, 2016, **138**, 15790–15796.

32 X. Wang, X. Han, J. Zhang, X. Wu, Y. Liu and Y. Cui, *J. Am. Chem. Soc.*, 2016, **138**, 12332–12335.

33 J. Guo and D. Jiang, *ACS Cent. Sci.*, 2020, **6**, 869–879.

34 Q. Fang, J. Wang, S. Gu, R. B. Kaspar, Z. Zhuang, J. Zheng, H. Guo, S. Qiu and Y. Yan, *J. Am. Chem. Soc.*, 2015, **137**, 8352–8355.

35 L. Y. Bai, S. Z. F. Phua, W. Q. Lim, A. Jana, Z. Luo, H. P. Tham, L. Z. Zhao, Q. Gao and Y. L. Zhao, *Chem. Commun.*, 2016, **52**, 4128–4131.

36 N. Huang, L. Zhai, H. Xu and D. Jiang, *J. Am. Chem. Soc.*, 2017, **139**, 2428–2434.

37 Q. Sun, B. Aguila, J. Perman, L. D. Earl, C. W. Abney, Y. Cheng, H. Wei, N. Nguyen, L. Wojtas and S. Ma, *J. Am. Chem. Soc.*, 2017, **139**, 2786–2793.

38 W. Ji, L. Xiao, Y. Ling, C. Ching, M. Matsumoto, R. P. Bisbey, D. E. Helbling and W. R. Dichtel, *J. Am. Chem. Soc.*, 2018, **140**, 12677–12681.

39 L. Wei, T. Sun, Z. Shi, Z. Xu, W. Wen, S. Jiang, Y. Zhao, Y. Ma and Y. B. Zhang, *Nat. Commun.*, 2022, **13**, 7936.

40 J. Wang and S. Zhuang, *Coord. Chem. Rev.*, 2019, **400**, 213046.

41 Y. Li, W. Chen, W. Hao, Y. Li and L. Chen, *ACS Appl. Nano Mater.*, 2018, **1**, 4756–4761.

42 L. He, S. Liu, L. Chen, X. Dai, J. Li, M. Zhang, F. Ma, C. Zhang, Z. Yang, R. Zhou, Z. Chai and S. Wang, *Chem. Sci.*, 2019, **10**, 4293–4305.

43 Y. Li, C.-X. Yang, H.-L. Qian, X. Zhao and X.-P. Yan, *ACS Appl. Nano Mater.*, 2019, **2**, 7290–7298.

44 Q. Liao, C. Ke, X. Huang, G. Zhang, Q. Zhang, Z. Zhang, Y. Zhang, Y. Liu, F. Ning and K. Xi, *J. Mater. Chem. A*, 2019, **7**, 18959–18970.

45 S. Karak, K. Dey, A. Torris, A. Halder, S. Bera, F. Kanheerampockil and R. Banerjee, *J. Am. Chem. Soc.*, 2019, **141**, 7572–7581.

46 B. Garai, D. Shetty, T. Skorjanc, F. Gándara, N. Naleem, S. Varghese, S. K. Sharma, M. Baias, R. Jagannathan, M. A. Olson, S. Kirmizialtin and A. Trabolsi, *J. Am. Chem. Soc.*, 2021, **143**, 3407–3415.

47 C. Li, P. Guggenberger, S. W. Han, W. L. Ding and F. Kleitz, *Angew. Chem., Int. Ed.*, 2022, **61**, e202206564.

48 X. Zhu, S. An, Y. Liu, J. Hu, H. Liu, C. Tian, S. Dai, X. Yang, H. Wang, C. W. Abney and S. Dai, *AIChE J.*, 2017, **63**, 3470–3478.

49 T. Xu, S. An, C. Peng, J. Hu and H. Liu, *Ind. Eng. Chem. Res.*, 2020, **59**, 8315–8322.

50 J. Fang, W. Zhao, M. Zhang and Q. Fang, *Acta Chim. Sin.*, 2021, **79**, 186–191.

51 X. Liu, H. Pang, X. Liu, Q. Li, N. Zhang, L. Mao, M. Qiu, B. Hu, H. Yang and X. Wang, *Innovation*, 2021, **2**, 100076.

52 D. Shen, J. Liu, H. Yang and S. Yang, *Chem. Lett.*, 2013, **42**, 1545–1547.

53 Y. Deng, Z. Zhang, P. Y. Du, X. M. Ning, Y. Wang, D. X. Zhang, J. Liu, S. T. Zhang and X. Q. Lu, *Angew. Chem., Int. Ed.*, 2020, **59**, 6082–6089.

54 Z. Song, L. Miao, L. Li, D. Zhu, L. Gan and M. Liu, *Carbon*, 2021, **180**, 135–145.

55 H. Duan, Z. Song, L. Miao, L. Li, D. Zhu, L. Gan and M. Liu, *J. Mater. Chem. A*, 2022, **10**, 9837–9847.

56 Q. Liao, C. Ke, X. Huang, D. Wang, Q. Han, Y. Zhang, Y. Zhang and K. Xi, *Angew. Chem., Int. Ed.*, 2021, **60**, 1411–1416.

57 Y. Qin, L. Miao, M. Mansuer, Ch. Hu, Y. Lv, L. Gan and M. Liu, *ACS Appl. Mater. Interfaces*, 2022, **14**, 33328–33339.

58 Z. Song, L. Miao, L. Ruhlmann, Y. Lv, D. Zhu, L. Li, L. Gan and M. Liu, *Adv. Funct. Mater.*, 2022, **32**, 2208049.

59 S. T. Zhuang, R. Chen, Y. Liu and J. Wang, *J. Hazard. Mater.*, 2020, **385**, 121596.

60 S. Xue, B. Tu, Z. Li, X. Ma, Y. Xu, M. Li, C. Fang and H. Tao, *Colloids Surf., A*, 2021, **618**, 126489.

61 M. S. Tehrani and R. Zare-Dorabei, *RSC Adv.*, 2016, **6**, 27416–27425.

62 X. Zhuang, Y. Wan, C. Feng, Y. Shen and D. Zhao, *Chem. Mater.*, 2009, **21**, 706–716.

63 S. Xing, Q. Bing, L. Song, G. Li, J. Liu, Z. Shi, S. Feng and R. Xu, *Chem.–Eur. J.*, 2016, **22**, 16230–16235.

64 A. Jain, R. Balasubramanian and M. P. Srinivasan, *Chem. Eng. J.*, 2015, **273**, 622–629.

65 Q. Jiang, H. Huang, Y. Tang, Y. Zhang and C. Zhong, *Ind. Eng. Chem. Res.*, 2018, **57**, 15114–15121.

66 X. Zhu, S. An, Y. Liu, J. Hu, H. Liu, C. Tian, S. Dai, X. Yang, H. Wang, C. W. Abney and S. Dai, *AIChE J.*, 2017, **63**, 3470–3478.

67 H. J. Zhang, J. H. Wang, Y. H. Zhang and T. L. Hu, *J. Polym. Sci., Part A: Polym. Chem.*, 2017, **55**, 1329–1337.

68 P. Sun, L. Xu, J. Li, P. Zhai, H. Zhang, Z. Zhang and W. Zhu, *Chem. Eng. J.*, 2018, **334**, 377–388.

69 Q. Li, Z. Zhan, S. Jin and B. Tan, *Chem. Eng. J.*, 2017, **326**, 109–116.